Kinetics of Optical Properties of Colorectal Muscle During Optical Clearing

Isa Carneiro, Sónia Carvalho, Rui Henrique, Luís Oliveira, and Valery V. Tuchin

***Abstract*—In this paper, we describe a simple and indirect method to evaluate the kinetics of the optical properties for biological tissues under optical clearing treatments. We use the theoretical formalism in this method to process experimental data obtained from colorectal muscle samples to evaluate and characterize the dehydration and refractive index matching mechanisms.**

***Index Terms*—Colorectal muscle, kinetics of optical properties, optical clearing, refractive index kinetics.**

I. Introduction

THE optical immersion clearing method is extensively used in research nowadays to control the optical properties of biological tissues and cells, improve light propagation and reach higher tissue depths or increase image contrast and enhance fluorescence transport [1]–[4]. The method consists of partial replacement of tissue water by an agent with higher refractive index (RI), better matched to the RI of the other tissue components (designated as scatterers), temporal and reversible tissue dehydration accompanied by its shrinkage and better ordering of scatterers, to reduce light scattering [5].

When an *ex vivo* biological tissue sample is immersed in a solution containing an osmotic optical clearing agent (OCA), an osmotic pressure is created over the tissue sample [6]. As a result of this pressure, the free water in the interstitial locations of the tissue will flow out, allowing the approach of scatterers (tissue shrinkage), creating a short-term increase in the scattering coefficient (μ_s). In spite of some elevation of the μ_s, due to decreased sample thickness and better ordering (packing) of tissue components, optical transmittance increases [5]. With the water flux out, the OCA molecules in the immersing solution find it easier to diffuse into the interstitial locations of the tissue. They will partially replace the water of the tissue and force the scatterers to separate again (tissue swelling) [7]. The water loss by the tissue and the OCA diffusion to the interstitial space are the driving forces of the optical clearing (OC) mechanisms: tissue dehydration and RI matching [2], [6], [8]–[15].

Ideally, for the tissue to be completely transparent, the RI of the intestinal fluid (ISF), n_{ISF}, should reach the RI of the scatterers, n_{s}. In such a case, the relative RI (m), characterizing scattering efficiency would be 1 [9]:

$$m = \frac{n_s}{n_{ISF}}, \tag{1}$$

and the reduced (or transport) scattering coefficient, expressed as [16], [17]:

$$\mu_s' = \mu_s\,(1-g) = 3.28\pi a^2 \rho_s \left(\frac{2\pi n_{ISF}\, a}{\lambda_0}\right)^{0.37} (m-1)^{2.09}, \tag{2}$$

would be equal to zero. This equation is valid in the visible and NIR range for the system of noninteracting scatterers with a mean diameter $2a$ ($g > 0.9$, $5 < 2\pi a/\lambda < 50$, $1 < m < 1.1$); and where g is the scattering anisotropy factor; ρ_s is the volume density of the scattering centers; λ is the irradiating light wavelength [16].

For short-time OC treatments, such as 30 min, total scattering reduction is not possible. This fact has to do with the nature of water in the tissues, which have free and bound water. Free water is able to move when stimulated, but bound water is strongly connected to the other tissue components and cell organelles [18]. For bound water to convert into free water and consequently flow out from the tissue, a strong or long-term stimulation is necessary [7], [18], [19]. Free water is located both in the ISF and inside tissue cells, and to move it from cells to the outside through the ISF a strong osmotic pressure is necessary. For short-term treatments with low osmotic strength OCAs, only the free water in the ISF will flow out.

Since OC treatments are not intended to last many hours or days, it is necessary to evaluate and characterize their magnitude. One way to do it is to evaluate the RI kinetics of a tissue under OC treatment [7]. Another way is to evaluate the kinetics of the optical properties of the tissue or the kinetics of the scattering efficiency.

The evaluation of tissue RI kinetics can be made based only on collimated transmittance (T_{c}) and thickness measurements performed during the treatment, $d(t)$ [9]. By definition, T_{c} of a sample depends both on sample thickness (d) and on light

Manuscript received March 30, 2018; accepted May 20, 2018. Date of publication May 24, 2018; date of current version June 12, 2018. This work was supported by the Portuguese Grant FCT-UID/EQU/04730/2013. The work of Valery V. Tuchin was supported by the RF Government under Grant 14.Z50.31.0044. *(Luís Oliveira and Valery V. Tuchin contributed equally to this work.) (Corresponding author: Luís Oliveira.)*

I. Carneiro, S. Carvalho, and R. Henrique are with the Department of Pathology and Cancer Biology, and Epigenetics Group—Research Center, Portuguese Oncology Institute of Porto, Porto 4200-072, Portugal (e-mail: isa_carneiro@hotmail.com; soniadiasdecarvalho@gmail.com; henrique@ipoporto.min-saude.pt).

L. Oliveira is with the CIETI/Department of Physics, Polytechnic of Porto—School of Engineering, Porto 4200-072, Portugal (e-mail: lmo@isep.ipp.pt).

V. V. Tuchin is with the Research-Educational Institute of Optics and Biophotonics, Saratov State University, Saratov 410012, Russia, and the Interdisciplinary Laboratory of Biophotonics, Tomsk State University, Tomsk 634050, Russia (e-mail: tuchinvv@mail.ru).

Color versions of one or more of the figures in this paper are available online at http://ieeexplore.ieee.org.

Digital Object Identifier 10.1109/JSTQE.2018.2840346

attenuation coefficient, μ_t [8]:

$$T_c = e^{-\mu_t \times d}. \tag{3}$$

Since μ_t is the sum of μ_s and the absorption coefficient, μ_a, and if we assume that μ_a remains unchanged during the treatment, we can estimate $\mu_s(t)$ from $T_c(t)$ and $d(t)$. The assumption that μ_a remains unchanged during treatment is reasonable, since in biological tissues, the order of magnitude of μ_s is significantly higher than the order of magnitude of μ_a [20]–[23]. On the other hand, since the OC treatment leads to the partial replacement of interstitial water by an OCA with typically low absorption but with high refractive properties, the increase in the RI of the interstitial space will perform the RI matching mechanism, that ultimately will reduce only the light scattering in the tissue.

Once $\mu_s(t)$ of the tissue is obtained, the time dependence for the RI of ISF, $n_{ISF}(t)$, can be calculated as [7]:

$$n_{ISF}(t) = \frac{n_s}{\left(\sqrt{\frac{\mu_s(t)\times d(t)}{\mu_s(t=0)\times d(t=0)}} \times \left(\frac{n_s}{n_{ISF}(t=0)} - 1\right) + 1\right)}, \tag{4}$$

where n_s represents the RI of tissue scatterers, which remains unchanged during the treatment; $\mu_s(t=0)$ and $d(t=0)$ are the scattering coefficient and sample thickness for the natural tissue, before treatment is applied. The RI of ISF in natural sample is represented by $n_{ISF}(t=0)$ [7], [9].

The calculation indicated in (4) is made for individual wavelengths, but provided that spectral data is available, a specially designed software can reproduce $n_{ISF}(\lambda, t)$.

Once $n_{ISF}(t)$ is calculated, the time dependence for the RI of the entire tissue, $n_{tissue}(t)$, can be calculated through Gladstone and Dale equation [7], [9], [24]–[27]:

$$n_{tissue}(t) = f_{ISF}(t) \cdot n_{ISF}(t) + f_s(t) \cdot n_s.$$
$$f_{ISF}(t) + f_s(t) = 1 \tag{5}$$

If the sample used in the treatment has a slab form with superficial area much larger than its thickness, the volume fractions ($f_{ISF}(t)$ and $f_s(t)$) in (5) can be determined from the thickness measurements performed during treatment. Once again, the calculation indicated in (5) can be performed for various wavelengths to obtain $n_{tissue}(\lambda, t)$.

Colorectal cancer is a source of major concern since it has high incidence worldwide [28]. Adenomatous polyps begin their development in the colorectal mucosa (see Fig. 1). They can evolve into invasive carcinoma and grow into deeper layers of the colorectal wall, reaching the submucosa, the muscle layer or eventually adjacent organs. Because of such development sequence, and with the objective of guiding future clinical decisions and possible treatments, the colorectal muscle layer is also of interest to study.

Noninvasive optical technologies to remove colorectal cancer are desired and significant research has been made recently in this field [29]–[31]. Due to the distinct tissue layers in colorectal wall, OC treatments can be used to increase light penetration depth and allow removal of entire polyp.

To evaluate OC treatments in the muscle layer of colorectal wall, we have used this tissue to measure $d(t)$ and $T_c(\lambda, t)$ during treatment with 40%-glycerol, and calculate the kinetics for its RI and optical properties.

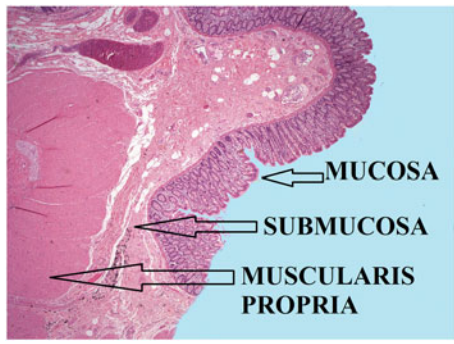

Fig. 1. Histology photograph of the colorectal wall showing the various layers – mucosa, submucosa and muscularis propria.

Fig. 2. Thickness measuring setup.

II. Materials and Methods

A. Tissue Collection and Preparation

All the tissue samples used in this study were surgically resected from 4 adult patients under treatment at the Oncology Institute of Porto (Portugal), after they signed a written consent, allowing for the use of surgical specimens for research purposes. The muscle layers were retrieved from the colorectal wall and fractioned into smaller pieces for later preparation. These smaller pieces were preserved frozen at −80 °C for a period of 12 to 24 h, before being sliced with a cryostat (Leica model CM 1850 UV) into a set of 6 circular slab-form samples ($\phi = 1$ cm, $d = 0.5$ mm) to use in our study.

B. Thickness Measurements

Three of the samples were used to evaluate $d(t)$ during OC treatment with 40%-glycerol solution. Each of these samples was placed inside two microscope glasses (thickness, D = 1 mm) and the treating solution was injected in-between the glasses to immerse the tissue sample (see Fig. 2). Global thickness of this setup was measured with a precise micrometer during 30 min treatment.

After completing measurements, the glasses thickness was subtracted from the registered measurements to obtain $d(t)$. Mean of $d(t)$ was calculated from the three studies.

C. T_c Measurements

Three studies were performed to acquire muscle's T_c spectra during 30 min treatment with 40%-glycerol. In each of these studies an individual muscle sample was immersed in the treating solution and spectra were collected between 400 and 1000 nm. Fig. 3 presents the setup used in these measurements.

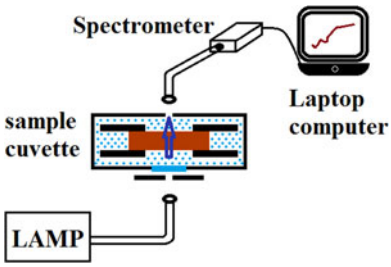

Fig. 3. T_c measuring setup.

A Deuterium-Halogen lamp was used to irradiate the sample through an optical fiber cable and collimating lens. A 1 mm pinhole is placed below the lower glass (in blue in Fig. 3) represented in the setup. The sample cuvette maintains the treating solution above and below the sample to keep it immersed (blue dots in Fig. 3). After crossing the sample, the beam passes through another 1 mm pinhole, before it is collected by lens and optical fiber to deliver to the spectrometer. Spectra are stored on laptop computer.

At the end of studies, the average for $T_c(\lambda, t)$ was calculated.

D. RI and Optical Properties Kinetics Calculation

We have previously estimated the wavelength dependencies for the optical properties of colorectal muscle [23] and its free water content as 60% [32]. Such data was used in calculations and are presented in section III.

Since the ISF contains both free and bound water, we needed to estimate the correct dispersions for scatterers, $n_s(\lambda)$ and ISF, $n_{ISF}(\lambda)$. By combining the dispersions of dry proteins and water [7] in both terms of (5) to match the colorectal dispersion, we obtained $n_s(\lambda)$ and $n_{ISF}(\lambda)$.

Considering a particular wavelength, λ_1, to calculate $n_{ISF}(\lambda_1, t)$, we first used $T_c(\lambda_1, t)$ and $d(t)$ in a rearranged version of (3). This calculation gave $\mu_t(\lambda_1, t)$. By subtracting $\mu_a(\lambda_1, t = 0)$ to $\mu_t(\lambda_1, t)$, we obtained $\mu_s(\lambda_1, t)$. Using the estimated data for $\mu_s(\lambda_1, t = 0)$, $d(t = 0)$, $\mu_s(\lambda_1, t)$, $d(t)$, $n_s(\lambda_1)$ and $n_{ISF}(\lambda_1, t = 0)$ in (4), we calculated $n_{ISF}(\lambda_1, t)$. This procedure was repeated for several wavelengths between 400 and 1000 nm.

To combine $n_{ISF}(\lambda, t)$ with $n_s(\lambda)$ in (5) and obtain $n_{tissue}(\lambda, t)$, we needed to calculate $f_{ISF}(t)$ and $f_s(t)$. Since the scatterers in natural colorectal muscle are a combination of proteins and bound water, we considered a model that accounts only for free water flux out of the tissue during dehydration. From the previously estimated free water content of 60% [32], we considered for natural tissue: $f_{ISF}(t = 0) = 0.6$ and $f_s(t = 0) = 0.4$.

Bearing in mind that the muscle samples had a circular slab form, we have first calculated their volume as:

$$V_{sample}(t = 0) = \left(\pi \times 0.5^2\right) \times 0.05\,\mathrm{cm}^3. \tag{6}$$

Then, we calculated the absolute volume of scatterers in natural tissue as 40% of the V_{sample}:

$$V_{scat} = V_{sample}\,(t = 0) \times 0.4\,\mathrm{cm}^3. \tag{7}$$

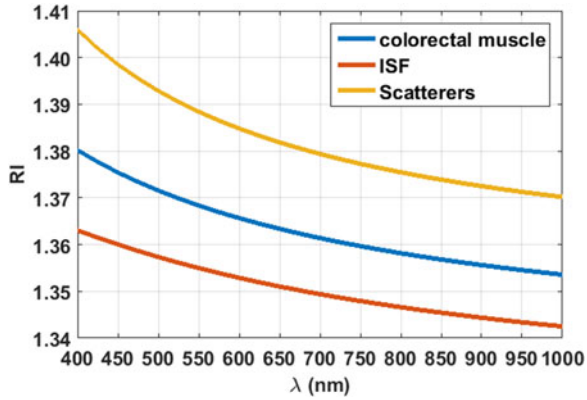

Fig. 4. Dispersions for colorectal muscle, its ISF and scatterers.

This volume will remain unchanged during treatment, while its volume fraction (VF) changes accordingly to:

$$f_{scat}\,(t) = \frac{V_{scat}}{\left(\pi \times 0.5^2\right) \times d\,(t)}. \tag{8}$$

Since for any time of treatment, the sum of all VFs must be 1, the VF of ISF is calculated as:

$$f_{ISF}\,(t) = 1 - f_{scat}\,(t)\,. \tag{9}$$

After obtaining $f_{scat}(t)$ and $f_{ISF}(t)$, we could use (5) to calculate $n_{tissue}(\lambda, t)$.

To calculate the kinetics of the optical properties of the colorectal muscle, we started by using a corrected form of (10) to estimate the mean particle radius, *a*, of the supposed spherical particle scatterers [16]:

$$\mu_s' = \frac{3 f_{scat}\,(1 - f_{scat})}{4\pi a^3} \times 3.28\pi a^2 \left(\frac{2\pi a n_{ISF}}{\lambda}\right)^{0.37} (m - 1)^{2.09}. \tag{10}$$

In this calculation, we used data from the natural muscle: μ_s' as obtained from IAD simulations and *m* obtained from (1). The mean *a* value for the wavelength range between 400 and 1000 nm was 5×10^{-7} m, which was later fixed in (10) to use with $n_{ISF}(\lambda, t)$ and $m(\lambda,t)$ for calculation of $\mu_s'(\lambda, t)$.

Finally, using $\mu_s'(\lambda, t)$ and $\mu_s(\lambda, t)$ we calculated the time dependence for the anisotropy-factor, $g(\lambda, t)$ as:

$$g = 1 - \frac{\mu'_s}{\mu_s}. \tag{11}$$

The results of these calculations are presented in section III.

III. Results and Calculations

A. Optical Properties of Natural Muscle

As previously explained, we used (5) to estimate $n_s(\lambda, t = 0)$ and $n_{ISF}(\lambda, t = 0)$ in colorectal muscle. Fig. 4 presents these data, along with the experimental dispersion data for the tissue.

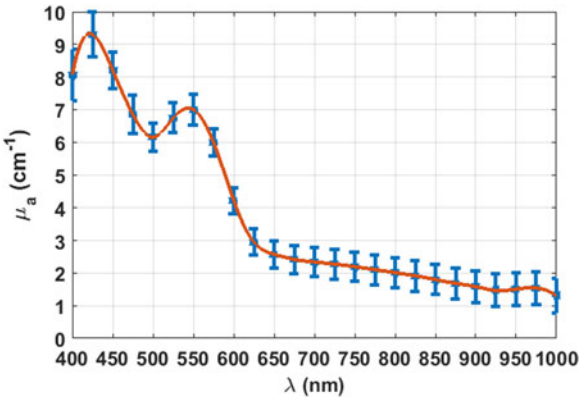

Fig. 5. Absorption coefficient $\mu_a(\lambda)$ for natural colorectal muscle.

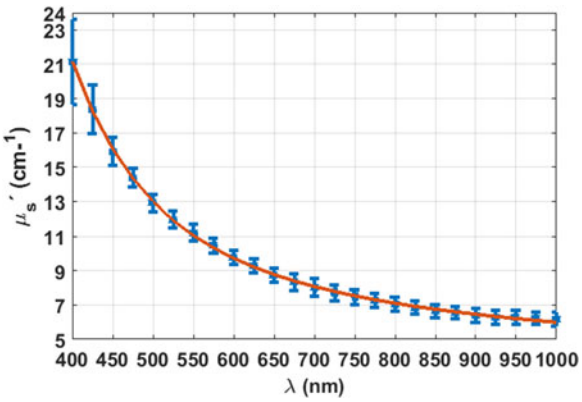

Fig. 6. Reduced scattering coefficient $\mu_s'(\lambda)$ for natural colorectal muscle.

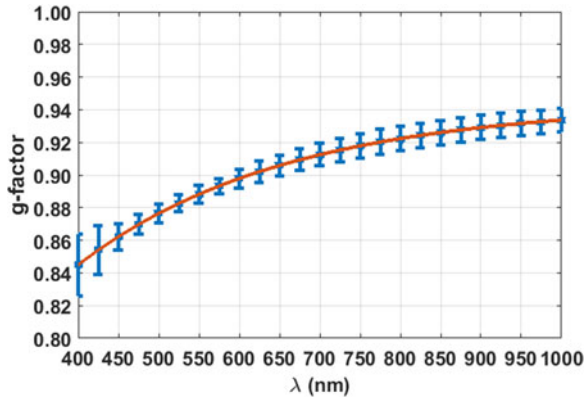

Fig. 7. Scattering anisotropy factor $g(\lambda)$ for natural colorectal muscle.

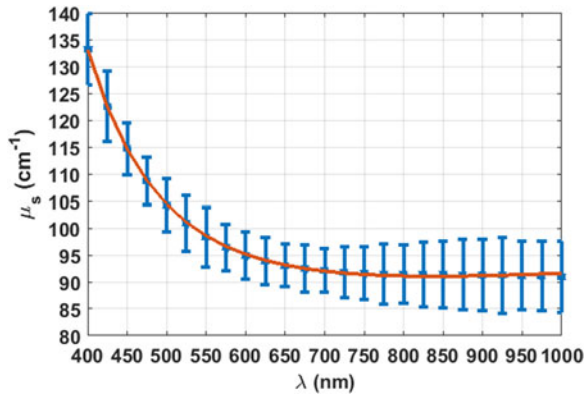

Fig. 8. Scattering coefficient $\mu_s(\lambda)$ for natural colorectal muscle.

The curves presented in Fig. 4 are described by:

$$n_{muscle}\left(\lambda\right) = 1.3346 + \frac{19.48}{\lambda + 27.17}, \tag{12}$$

$$n_{scatterers}\left(\lambda\right) = 1.3512 + \frac{17.42}{\lambda - 81.94}, \tag{13}$$

$$n_{ISF}\left(\lambda\right) = 1.321 + \frac{26.3}{\lambda + 223.7}. \tag{14}$$

As a result of 10 IAD simulations [23], [33], the mean wavelength dependencies for $\mu_a(\lambda, t = 0)$ and $\mu_s'(\lambda, t = 0)$ are presented in Fig. 5 and Fig. 6. Data in Fig. 8 was calculated with (3) from $T_c(\lambda, t = 0)$ and $d(t = 0)$ measurements – mean of 3 sets of measurements. Data for g in Fig. 7 was calculated using (11).

The bars in these graphs represent the standard deviation obtained from the various simulations or calculations at each wavelength. All optical properties show a wavelength dependence accordingly to literature [34]–[37].

The curve in Fig. 5 has no equation to describe it, and presents two absorption bands near 425 and 550 nm, which correspond to a mixture of oxy- and deoxy-hemoglobin bands of the blood in the muscle samples used [23], [38], [39].

For μ_s' we have calculated the curve in Fig. 6 with an $R^2 = 0.9995$ as:

$$\mu_s'\left(\lambda\right) = 13.01 \times \left(0.3859 \times \left(\frac{\lambda}{500(\text{nm})}\right)^{-4} + 0.6141 \times \left(\frac{\lambda}{500(\text{nm})}\right)^{-0.4927}\right). \tag{15}$$

The curve in Fig. 7 was obtained with an $R^2 = 0.9993$ as:

$$g\left(\lambda\right) = 0.3432 + 0.6003 \times \left(1 - e^{-\frac{\lambda+70}{260}}\right). \tag{16}$$

The curve in Fig. 8 was estimated with an $R^2 = 0.9995$ as:

$$\mu_s\left(\lambda\right) = 104.4 \times \left(0.2059 \times \left(\frac{\lambda}{500(\text{nm})}\right)^{-4} + 0.7941 \times \left(\frac{\lambda}{500(\text{nm})}\right)^{0.123}\right). \tag{17}$$

Literature [37], [40] presents these equations as adequate to fit $g(\lambda)$, $\mu_s'(\lambda)$ and $\mu_s(\lambda)$. A mixed combination of Rayleigh and Mie scattering terms is accounted in (15) and (17) [40].

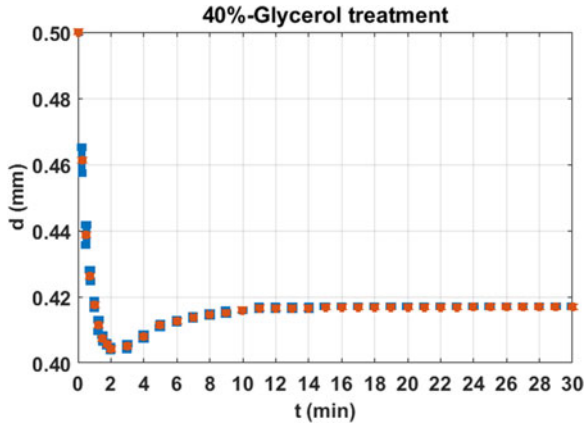

Fig. 9. Mean time dependence of sample thickness during treatment.

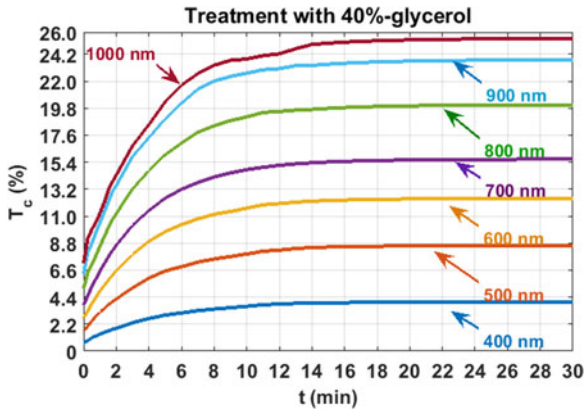

Fig. 10. Mean Tc time dependence of colorectal muscle at some wavelengths during treatment with 40%-glycerol.

B. Thickness and Tc Measurements During Treatment

The mean $d(t)$, calculated from the three sets of measurements, is presented in Fig. 9, showing a considerable decrease within the first 2 min of treatment. This initial decrease indicates the dehydration of the sample.

After 2 min of treatment, d increases in a smooth manner, translating the diffusion of glycerol molecules into the sample. Such behavior tends to become stable after 16 min, meaning that no effective flux occurs after that time.

The higher magnitude error bars at the beginning of treatment in Fig. 9 indicate a more compressible sample and more favorable for errors to occur in measurements.

The mean T_c time dependence is presented in Fig. 10 for some wavelengths:

Similar uncertainty for all the curves presented in Fig. 10 was $\sim$4% of the represented values within the first 4 min and $\sim$2.4% after that time. The smooth behavior in these curves translates the diffusion of glycerol molecules with a good accuracy. For this particular solution, a balance is established between the free water in the tissue and the water in the solution. As a result, no effective water flux occurs during treatment [6], [15], [32], [41].

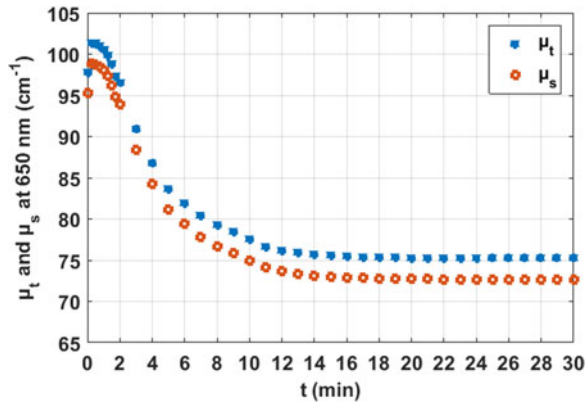

Fig. 11. Time dependencies for μ_t and μ_s at 650 nm.

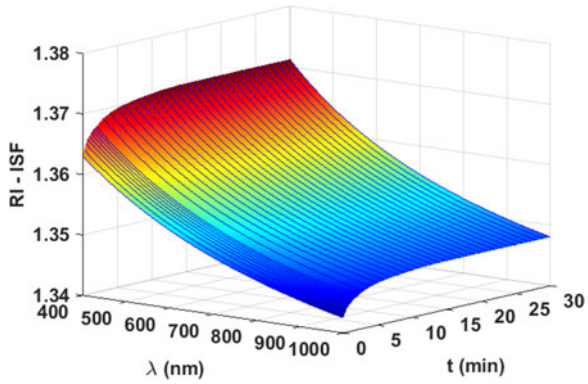

Fig. 12. Time dependency for the mean RI of ISF.

C. Calculation of the RI Kinetics

To determine $n_{ISF}(\lambda, t)$ for colorectal muscle, we started by calculating $\mu_t(\lambda, t)$ with (3). From $\mu_t(\lambda, t)$ we calculated $\mu_s(\lambda, t)$ by subtracting $\mu_a(\lambda, t = 0)$. This calculation was performed for various wavelengths between 400 and 1000 nm. Fig. 11 presents $\mu_t(t)$ and $\mu_s(t)$ at 650 nm, where we see an overall decrease for both coefficients as a result of the treatment.

The small initial increase in μ_s and μ_t at the beginning of treatment is evidence of the dehydration mechanism – scatterers approach each-other as a result of the water loss, leading to the observed momentary increase. The smooth overall decrease seen in Fig. 11 for both coefficients is driven mainly by the T_c data.

The following calculation step was to obtain $n_{ISF}(\lambda, t)$ with (4). The resultant time dependence is presented in Fig. 12.

Fig. 12 shows a smooth increase in n_{ISF}, very similar to the behavior observed for T_c in Fig. 10, indicating that the T_c measurements are sensitive to the changes in n_{ISF}. At the end of treatment, n_{ISF} does not match n_s (see Fig. 4), indicating that the pressure created by glycerol was not strong enough to move the free water inside the cells to the outside through the ISF.

Fig. 13 presents the time dependence for $m(\lambda, t)$, as calculated from $n_{ISF}(\lambda, t)$ and $n_s(\lambda)$ using (1).

We see from Fig. 13 that although reduction in m is not total, it occurs in a smooth way for all wavelengths.

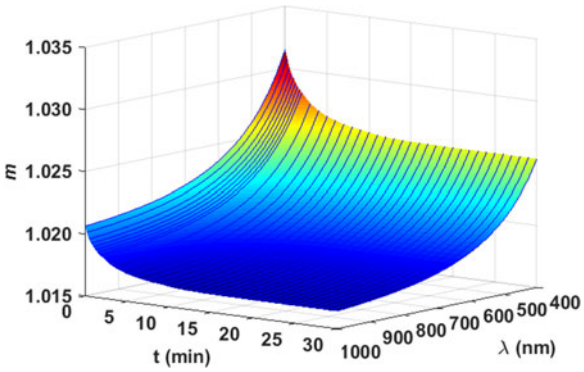

Fig. 13. Relative index of refraction $m(\lambda, t)$, characterizing scattering efficiency during treatment.

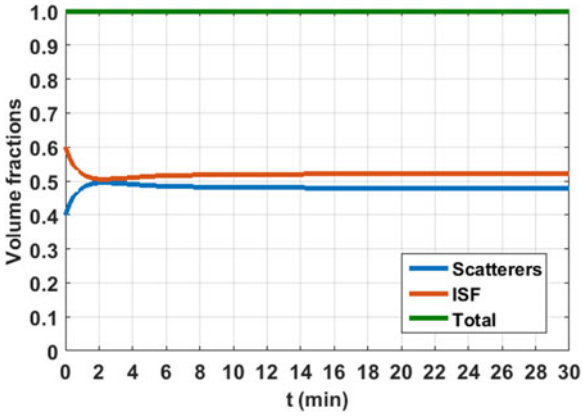

Fig. 14. Time dependence for the volume fractions of colorectal muscle's components during treatment with 40%-glycerol.

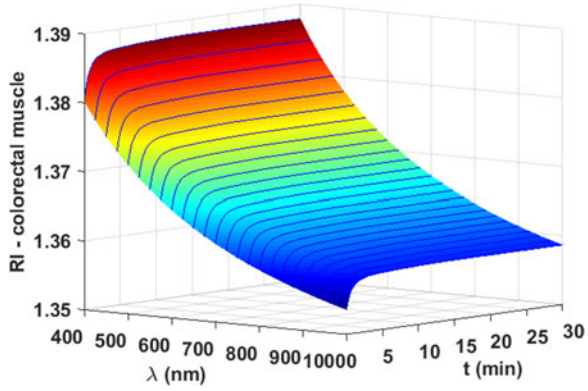

Fig. 15. Time dependence for the dispersion of colorectal muscle between 400 and 1000 nm during treatment with 40%-glycerol.

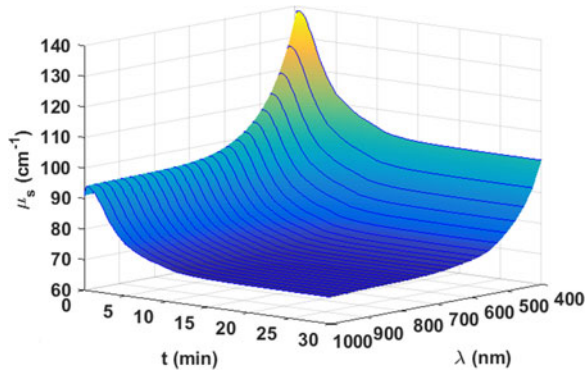

Fig. 16. Time dependence for the $\mu_s(\lambda, t)$ of colorectal muscle between 400 and 1000 nm during treatment with 40%-glycerol.

With this data, we can calculate $n_{\text{tissue}}(\lambda, t)$ for the colorectal muscle. To perform this calculation with (5), we have first calculated $f_{\text{scat}}(t)$ and $f_{\text{ISF}}(t)$ with (8) and (9). These time dependencies are presented in Fig. 14, where a significant and fast variation in VFs is seen within the first 2 min. This means that tissue dehydration dominates at this early stage of treatment (see Fig. 9). After 3 min, smooth and low magnitude variations are observed for the VFs, meaning that they are now driven by the RI matching mechanism in the ISF. In other words, the two OC mechanisms can be detected in Fig. 14.

To finalize calculations, we used (4) to calculate $n_{\text{tissue}}(\lambda, t)$. The result of this calculation is presented in Fig. 15.

In Fig. 15 we see three stages: within the first min, a strong increase in n_{tissue} corresponds to the dehydration mechanism; the following 3 min correspond to a transition between mechanisms; and following 26 min correspond uniquely to the RI matching mechanism.

The data in Fig. 15 shows that since glycerol has no strong absorption bands in this wavelength range, it produces similar efficiency in the entire spectral range.

D. Calculation of Kinetics of the Optical Properties

We now present the kinetics of the optical properties for colorectal muscle.

The calculations performed in the previous section have also produced data for $\mu_s(\lambda, t)$, as already presented in Fig. 11 for 650 nm. The entire 3-D map is presented in Fig. 16.

Fig. 16 shows a small increase in μ_s at the beginning of the treatment, but the overall effect is a smooth major decrease in μ_s for all wavelengths. The initial increase is due to scatterers approaching each-other as water flows out during dehydration. We have not seen this effect in Fig. 10 due to the fact that d also decreases at the early stage of treatment, leading to an increase in T_c.

Using (10) for the various times of treatment, we have also calculated $\mu'_s(\lambda, t)$. Fig. 17 presents its 3-D map, where μ'_s presents similar time dependence to m (see Fig. 14) – it decreases smoothly for all wavelengths.

Finally, we used (11) to calculate $g(\lambda, t)$ from the data in Fig. 16 and Fig. 17. As expected, we see an increase in g over time for all wavelengths – Fig. 18.

At the beginning of treatment, the increase is strong and fast and, indicating that the water loss leads to a better packing inside the tissue. Therefore, forward scattering increases.

We see a small decrease in g after 2 min due to the transition between the dehydration and RI matching mechanisms, since OCA molecules start to force the scatterers to separate from each-other (see Fig. 14).

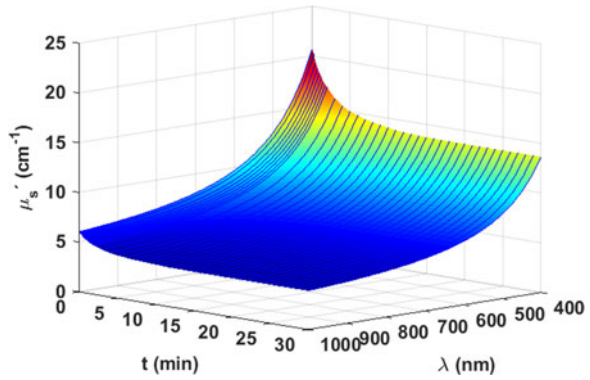

Fig. 17. Time dependence for the $\mu_s'(\lambda, t)$ of colorectal muscle between 400 and 1000 nm during treatment with 40%-glycerol.

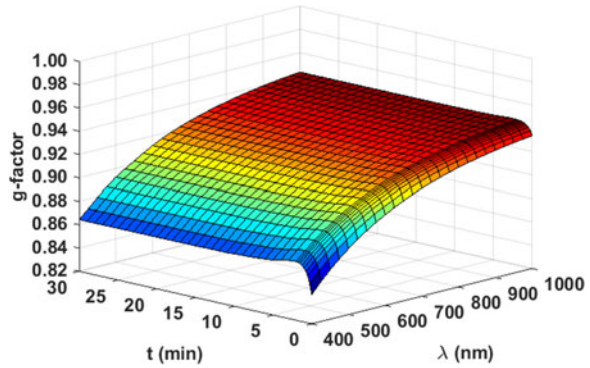

Fig. 18. Time dependence for the g-factor of colorectal muscle between 400 and 1000 nm during treatment with 40%-glycerol.

IV. Conclusion

A simple indirect method based on thickness and T_c measurements was used to evaluate the kinetics of the optical properties for colorectal muscle under treatment with 40%-glycerol. The results from this study show that this method is very sensitive to the two main OC mechanisms – tissue dehydration and RI matching. We have also observed that although the increase in the RI of the ISF of the tissue was not too high, it occurs in the same manner for the entire wavelength range of 400–1000 nm. Similar behavior was also observed for the other optical properties.

The 3-D maps for μ_s, μ_s' show a decrease and g shows an increase over the time of treatment, as expected. The evaluation of the magnitudes in these variations, or the time dependence of m are very valuable to characterize the treatment.

This method can be used to study other treatments of the colorectal muscle with different glycerol concentrations for comparison of for evaluating other OCAs in different tissues.

References

[1] V. V. Tuchin *et al.*, "Light propagation in tissues with controlled optical properties," *J. Biomed. Opt.*, vol. 2, no. 4, pp. 401–417, Oct. 1997.

[2] E. A. Genina, A. N. Bashkatov, and V. V. Tuchin, "Tissue optical immersion clearing," *Expert Rev. Med. Devices*, vol. 7, no. 6, pp. 825–842, Nov. 2010.

[3] D. Zhu, K. V. Larin, Q. Luo, and V. V. Tuchin, "Recent progress in tissue optical clearing," *Laser Photon. Rev.*, vol. 7, no. 5, pp. 732–757, Feb. 2013.

[4] A. Yu. Sdobnov *et al.*, "Recent progress in tissue clearing for spectroscopic application," *Spectrochim. Acta A, Mol. Biomol. Spectrosc.*, vol. 197, pp. 216–229, Feb. 3, 2018. pii: S1386-1425(18)30111-2. doi: 10.1016/j.saa.2018.01.085.

[5] L. Oliveira, M. I. Carvalho, E. Nogueira, and V. V. Tuchin, "Optical clearing mechanisms characterization in muscle," *J. Innov. Opt. Health Sci.*, vol. 9, no. 5, Apr. 2016, Art. no. 1650035.

[6] L. Oliveira, M. I. Carvalho, E. Nogueira, and V. V. Tuchin, "Diffusion characteristics of ethylene glycol in skeletal muscle," *J. Biomed. Opt.*, vol. 20, no. 5, May 2015, Art. no. 051019.

[7] L. Oliveira, M. I. Carvalho, E. Nogueira, and V. V. Tuchin, "Skeletal muscle dispersion (400-1000 nm) and kinetics at optical clearing," *J. Biophoton.*, vol. 11, no. 1, Jan. 2018, Art. no. e201700094.

[8] V. V. Tuchin, *Tissue Optics: Light Scattering Methods and Instruments for Medical Diagnosis*, 3rd ed. Bellingham, WA, USA: SPIE, 2015, ch.1 and ch. 9.

[9] V. V. Tuchin, *Optical Clearing of Tissues and Blood*. Bellingham, WA, USA: SPIE, 2006, ch.1.

[10] V. V. Tuchin, "Optical immersion as a new tool for controlling the optical properties of tissues and blood," *Laser Phys.*, vol. 15, no. 8, pp. 1109–1136, Aug. 2005.

[11] B. Choi *et al.*, "Determination of chemical agent optical clearing potential using in vitro human skin," *Lasers Surg. Med.*, vol. 36, no. 2, pp. 72–75, Feb. 2005.

[12] S. Plotnikov, V. Juneja, A. B. Isaacson, W. A. Mohler, and P. J. Campagnola, "Optical clearing for improved contrast in second harmonic generation imaging of skeletal muscle," *Biophys. J.*, vol. 90, no. 1, pp. 328–339, Oct. 2006.

[13] X. Wen, V. V. Tuchin, Q. Luo, and D. Zhu, "Controlling the scattering of intralipid by using optical clearing agents," *Phys. Med. Biol.*, vol. 54, no. 22, pp. 6917–6930, Nov. 2009.

[14] L. Oliveira, A. Lage, M. Pais Clemente, and V. V. Tuchin, "Rat muscle opacity decrease due to the osmosis of a simple mixture," *J. Biomed. Opt.*, vol. 15, no. 5, Sep. 2010, Art. no. 055004.

[15] L. Oliveira, M. I. Carvalho, E. Nogueira, and V. V. Tuchin, "The characteristic time of glucose diffusion measured for muscle tissue at optical clearing," *Laser Phys.*, vol. 23, no. 7, May 2013, Art. no. 075606.

[16] H. Liu, B. Beauvoit, M. Kimura, and B. Chance, "Dependence of tissue optical properties on solute-induced changes in refractive index and osmolarity," *J. Biomed. Opt.*, vol. 1, no. 2, pp. 200–211, Apr. 1996.

[17] R. Graaff *et al.*, "Reduced light-scattering properties for mixtures of spherical particles: A simple approximation derived from Mie calculations," *Appl. Opt.*, vol. 31, no. 10, pp. 1370–1376, Apr. 1992.

[18] V. Gillard *et al.*, "Measurement of total water and bound water content in human stratum corneum by in vitro proton nuclear magnetic resonance spectroscopy," *Int. J. Cosmet. Sci.*, vol. 20, no. 2, pp. 117–125, Apr. 1998.

[19] B. Schultz, D. Chan, J. Bäckström, and M. Rübhausen, "Spectroscopic ellipsometry on biological materials – investigation of hydration dynamics and structural properties," *Thin Solid Films*, vol. 455, pp. 731–734, May 2004.

[20] A. N. Bashkatov *et al.*, "Optical properties of human colon tissues in the 350-2500 nm spectral range," *Quantum Electron.*, vol. 44, no. 8, pp. 779–784, Aug. 2014.

[21] A. N. Bashkatov, E. A. Genina, and V. V. Tuchin, "Optical properties of skin, subcutaneous, and muscle tissues: A review," *J. Innov. Opt. Health Sci.*, vol. 4, no. 1, pp. 9–38, Jan. 2011.

[22] S. Carvalho *et al.*, "Comparative study of the optical properties of colon mucosa and colon precancerous polyps between 400 and 1000 nm," *Proc. SPIE*, vol. 100631L, Jan. 2017, Art. no. 100631L.

[23] I. Carneiro, S. Carvalho, R. Henrique, L. Oliveira, and V. V. Tuchin, "Optical properties of colorectal muscle in visible/NIR range," in *Proc. SPIE—Photon. Europe*, 2018, Paper 106853D.

[24] D. W. Leonard and K. M. Meek, "Refractive indices of the collagen fibrils and extrafibrillar material of the corneal stroma," *Biophys. J.*, vol. 72, no. 3, pp. 1382–1387, Mar. 1997.

[25] K. M. Meek, S. Dennis, and S. Khan, "Changes in the refractive index of the stroma and its extrafibrillar matrix when the cornea swells," *Biophys. J.*, vol. 85, no. 4, pp. 2205–2212, Oct. 2003.

[26] K. M. Meek, D. W. Leonard, C. J. Connon, S. Dennis, and S. Khan, "Transparency, swelling and scarring in the corneal stroma," *Eye*, vol. 17, no. 8, pp. 927–936, Nov. 2003.

[27] O. Zhernovaya, O. Sydoruk, V. V. Tuchin, and A. Douplik, "The refractive index of human hemoglobin in the visible range," *Phys. Med. Biol.*, vol. 56, no. 13, pp. 4013–4021, Jul. 2011.
[28] H. Brenner, M. Kloor, and C. P. Pox, "Colorectal cancer," *Lancet*, vol. 383, pp. 1490–1502, Nov. 2013.
[29] P. C. Lopes *et al.*, "Discriminating adenocarcinoma from normal colonic mucosa through deconvolution of Raman spectra," *J. Biomed. Opt.*, vol. 16, no. 12, Dec. 2011, Art. no. 127001.
[30] M. V. P. Chowdary *et al.*, "Discrimination of normal and malignant mucosal tissues of the colon by Raman spectroscopy," *Photomed. Laser Surg.*, vol. 25, no. 4, pp. 269–274, Aug. 2007.
[31] D. Hirović-Rowe and E. Claridge, "Modeling and validation of spectral reflectance for the colon," *Phys. Med. Biol.*, vol. 50, no. 6, pp. 1071–1093, Feb. 2005.
[32] I. Carneiro, S. Carvalho, R. Henrique, L. Oliveira, and V. V. Tuchin, "Water content and scatterers dispersion evaluation in colorectal tissues," *J. Biomed. Photon. Eng.*, vol. 3, no. 4, Dec. 2017, Art. no. 04301.
[33] S. A. Prahl, M. J. C. van Gemert, and A. J. Welsh, "Determining the optical properties of turbid media by using the adding-doubling method," *Appl. Opt.*, vol. 32, no. 4, pp. 559–568, Feb. 1993.
[34] A. N. Bashkatov, E. A. Genina, V. I. Kochubei, and V. V. Tuchin, "Optical properties of human skin, subcutaneous and mucous tissues in the wavelength range from 400 to 2000 nm," *J. Phys. D, Appl. Phys.*, vol. 38, no. 15, pp. 2543–2555, Jul. 2005.
[35] A. N. Bashkatov *et al.*, "Optical properties of human stomach mucosa in the spectral range from 400 to 2000 nm: Prognosis for gastroenterology," *Med. Laser Appl.*, vol. 22, pp. 95–104, 2007.
[36] A. N. Bashkatov, E. A. Genina, V. I. Kochubei, and V. V. Tuchin, "Optical properties of the subcutaneous adipose tissue in the spectral range 400–2500 nm," *Opt. Spectrosc.*, vol. 99, no. 5, pp. 836–842, Nov. 2005.
[37] A. N. Bashkatov *et al.*, "Optical properties of peritoneal biological tissues in the spectral range of 350–2500 nm," *Opt. Spectrosc.*, vol. 120, no. 1, pp. 1–8, Jan. 2016.
[38] Mar. 27, 2018. [Online]. Available: http://omlc.org/spectra
[39] S. Takatani and M. D. Graham, "Theoretical analysis of diffuse reflectance from a two-layer tissue model," *IEEE Trans. Biomed. Eng.*, vol. 26, no. 12, pp. 656–664, Dec. 1979.
[40] S. L. Jacques, "Optical properties of biological tissues: A review," *Phys. Med. Biol.*, vol. 58, no. 11, pp. R37–R61, Jul. 2013.
[41] S. Carvalho *et al.*, "Glucose diffusion in colorectal mucosa–A comparative study between normal and cancer tissues," *J. Biomed. Opt.*, vol. 22, no. 9, Sep. 2017, Art. no. 091506.

Isa Carneiro received the B.Sc. degree in pathologic, cytologic and tanatologic anatomy from Porto Polytechnic Institute, Porto, Portugal, in 2008, and the M.S. degree in oncology from Porto University, Porto, in 2012.

She is a Technician of Pathological Anatomy with the Department of Pathology, Portuguese Oncology Institute of Porto, Porto. Her main research interest includes prostate cancer.

Dr. Carneiro is also a Member with the Cancer Biology and Epigenetics Group, Portuguese Oncology Institute of Porto Research Center.

Sónia Carvalho received the M.D. degree in medicine from the Faculty of Medicine, University of Coimbra, Coimbra, Portugal, in 2012.

She has started supervised medical practice in January 2013 and is currently a fifth-year Pathology Resident with the Portuguese Oncology Institute, Porto, Portugal. She participates in different medical and scientific activities within the scope of the residency program. Her main research interest incudes colorectal carcinoma.

Dr. Carvalho is a Member of the European and Portuguese Societies of Pathology.

Rui Henrique received the M.D. degree in 1992, the Ph.D. degree in medical sciences in 2006, and the Habilitation degree in pathology and molecular genetics in 2011, all from the Abel Salazar Institute of Biomedical Sciences, University of Porto (ICBAS-UP), Porto, Portugal.

He has been a Specialist of Pathology since 2001 and the Director with the Department of Pathology, Oncology Institute of Porto, Portugal, since 2006. He is an invited Full Professor with ICBAS-UP and coordinates and lectures pathology and anatomic pathology to the medical course, among others. He has authored/coauthored more than 190 publications in international peer-reviewed scientific periodicals, including book chapters, review papers, and original papers, with more than 4300 citations and *h*-index (Scopus) of 37. His research interests include the role of epigenetic alterations in urological cancers and the development of novel cancer biomarkers.

Luís Oliveira received the graduation degree in physics, the M.S. degree in biomedical engineering, and the Ph.D. degree in biomedical engineering from Porto University, Porto, Portugal, in 2000, 2010, and 2014, respectively.

Since 2001, he has been an optics researcher. Since 2008, he has been a Professor with the Department of Physics, Polytechnic of Porto—School of Engineering, Portugal. He is also a Biophotonics Researcher with the Center for Innovation in Engineering and Industrial Technology, a research center that is part of the Polytechnic of Porto. In recent years he has reviewed and authored several papers in the fields of tissue optics and tissue optical clearing. His research interests include tissue optics, tissue optical clearing and related applications, chemical diffusion in tissues, and optical properties control to develop new clinical methods.

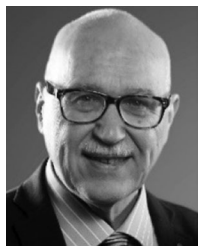

Valery V. Tuchin is a Professor and Head of Optics and Biophotonics with Saratov State University (National Research University of Russia), Saratov, Russia, and several other universities. His research interests include tissue optics, laser medicine, tissue optical clearing, and nanobiophotonics. He is a Fellow of SPIE and OSA. He was the recipient of the Honored Science Worker of the Russia, Honored Professor of Saratov University, SPIE Educator Award, FiDiPro (Finland), Chime Bell Prize of Hubei Province (China), and Joseph W. Goodman Book Writing Award (OSA/SPIE). He has 19246 citations and *h*-index 65 (Google Scholar, March 28, 2018).